I. Supplementary Information

CME's are driven by a release of magnetic energy, which dominates the interaction between the solar wind and CME in very low corona (<2 solar radii). When > 10 solar radii, solar wind and a CME is controlled by the drag force. (RM Evans, et al,2011)

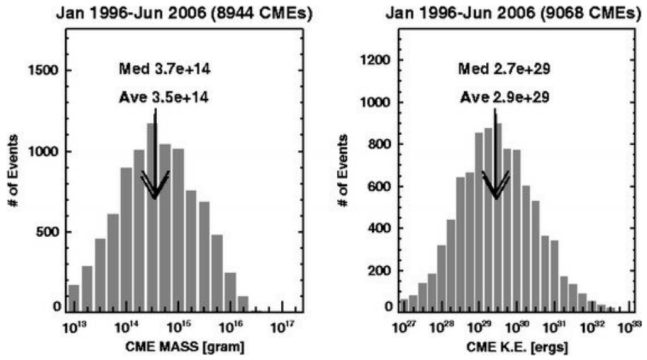

Figure. Distributions of CME mass and kinetic energy of all CMEs for which mass and speed measurements were possible with Kinetic Energy average of 2.9E29. (Gopalswamy, et al, 2009)

Date	Speed (km/s)	K.E. (Joules)	Mass (kilograms)
4/8/1996	316	1.1×10^{20}	2.2×10^{9}
8/22/2000	388	1.3×10^{22}	1.7×10^{11}
6/10/2001	731	8.2×10^{23}	3.1×10^{12}
1/18/2002	64	5.3×10^{19}	2.6×10^{10}
5/16/2002	1,310	6.7×10^{22}	7.8×10^{10}
10/7/2002	721	7.8×10^{21}	3.0×10^{10}
1/24/2003	387	9.1×10^{18}	1.2×10^{8}
10/31/2003	2,198	1.6×10^{24}	6.6×10^{11}
11/2/2003	2,033	9.3×10^{25}	4.5×10^{13}
11/10/2004	3,387	5.5×10^{25}	9.6×10^{12}

Table. CME Observational Data

The compact ejective flares in the reported events spanned only 10,000 km (or 1° in heliocentric angle), whereas the corresponding streamer-puff CMEs(narrow to moderate size) had angular widths of 20-40° (Moore and Sterling, 2007). Shocked background gas plays a dominant role in the propagation and subsequently the behavior of the plasma.Background gas and e- density expands as vapor plume by standard piston model. (Ma, et al, 2012)

Average X/O Ratios in High $\langle Q_{Fe} \rangle$ ICMEs and Other Solar Wind Plasmas Relative to the Photosphere[a]

	He/O	C/O	N/O	Ne/O	Mg/O	Si/O	S/O	Fe/O
Slow solar wind[b]	0.715	1.252	0.830	0.607	2.525	2.744	1.866	2.608
Errors	0.271	0.194	0.293	0.169	0.978	1.067	0.791	1.710
Fast solar wind[b]	0.581	1.380	1.146	0.523	1.849	1.925	1.866	1.753
Errors	0.064	0.121	0.252	0.124	0.462	0.477	0.506	0.513
High $\langle Q_{Fe} \rangle$ ICMEs	0.748	0.935	1.042	1.268	4.423	4.188	2.889	4.690
Error range min.	0.325	0.252	0.158	0.364	1.131	1.007	0.847	1.781
Error range max.	0.576	0.344	0.186	0.511	1.519	1.325	1.197	2.870
Other ICMEs	0.604	1.063	1.151	0.881	3.163	3.436	2.116	3.687
Error range min.	0.213	0.244	0.168	0.148	0.710	0.749	0.479	1.354
Error range max.	0.330	0.317	0.196	0.178	0.916	0.957	0.619	2.139

Notes.
[a] All values are normalized relative to the photospheric values of Grevesse & Sauval (1998).
[b] Average values for fast and slow wind from Von Steiger & Zurbuchen (2016).

Table. X/O ratios in high ICMEs and other solar wind plasmas Relative to Photosphere (Grevesse & Sauval 1998)

A large body of literature exists highlighting the rich data sets, which detail the unique charge composition observed within ICMEs (e.g., Zurbuchen & Richardson 2006; Zurbuchen et al. 2004; Lepri & Zurbuchen 2004; Lepri et al. 2001; Henke et al. 2001; Gloeckler et al. 1998; Henke et al. 1998, Galvin & Gloeckler 1997; Reinard 2005)

TABLE 1
ICME OBSERVATIONS

Year	Start (DOY)	v_{He++} (km s^{-1})[a]		ρ_{H+} (cm^{-3})		He/O[b]		Fe/O	
		Ave.	Max	Ave.	Max.	Ave.	Max.	Ave.	Max.
2002	173	416 ± 19	464	4.4 ± 1.1	6.9	80 ± 10	92	0.15 ± 0.03	0.19
2000	210	442 ± 34	474	15.1 ± 7.5	35.9	227 ± 245	1020	0.34 ± 0.31	0.90
2001	351	477 ± 20	500	3.6 ± 0.8	5.5	123 ± 16	147	0.06	0.07
2000	178	504 ± 42	569	5.2 ± 2.3	13.0	99 ± 38	171	0.21 ± 0.04	0.29
1998	268	640 ± 77	793	3.6 ± 2.2	11.1	100 ± 72	214	0.28 ± 0.13	0.56
2003	129	706 ± 78	855	3.2 ± 2.2	10.6	78 ± 27	114	0.18 ± 0.04	0.25
2000	262	718 ± 47	804	4.4 ± 3.1	13.3	222 ± 64	335	0.28 ± 0.17	0.67
2003	302	993 ± 305	1700	3.1 ± 1.9	9.2	168 ± 129	442	0.67 ± 0.42	2.33

[a] Ranges given are the standard deviation in the values over the ICME event and do not include uncertainties in the measurement.
[b] Ratio of the number densities of the given elements.

Table. ICME Observations(Rakowski, et al, 2007)

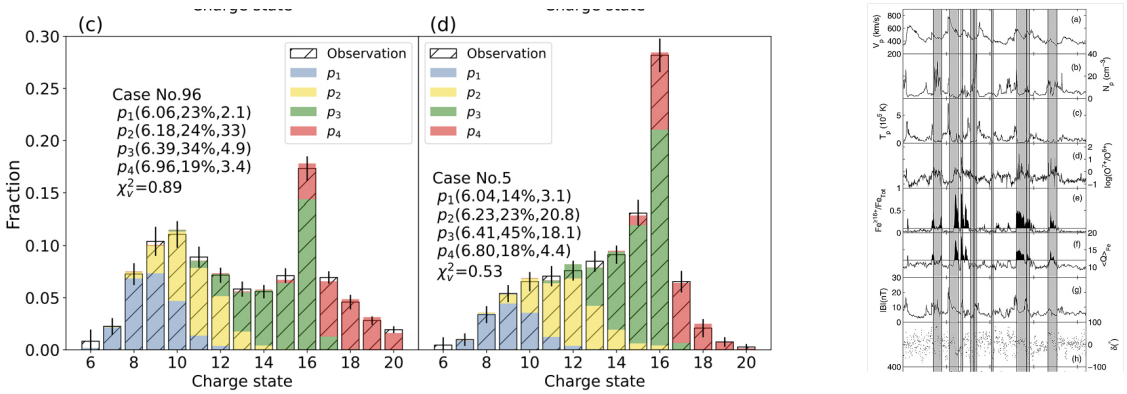

Figure. Measured and modeled charge-state distributions of iron ions of four selected ICMEs.(Gu, et al, 2023).

Averaged charge states of iron ions in ICMEs are highly related to the solar activity cycle. Authors propose that PC1 originates from prominence, PC2 is the common coronal plasma, and PC3 and PC4 are from the prominence–corona transition region.Eruptive prominences are associated with at least 70% of all CMEs and are often embedded within the bases of CME flux ropes.In steady state solar wind conditions, Fe charge states freeze in within 3–5 R⊙ from the Sun and remain unchanged as the particles travel through interplanetary space. Others estimated that iron ions freeze in at heights of ~5 solar radii.(Gu, et al, 2023). In comparing Fe charge state data from the ACE spacecraft, close to solar maximum, there is almost an order of magnitude fewer hot ICMEs at higher latitudes than in the ecliptic. We offer an explanation for the existence of high Fe charge states in hot ICMEs as a result of magnetic connectivity to flaring regions.(lepri, et al, 2004).

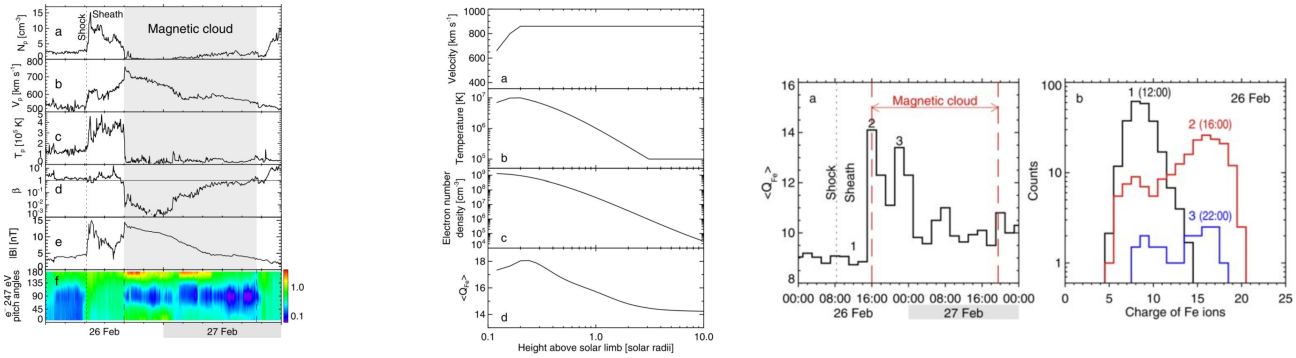

Figure. ICME produced by the 24 February 2011 event as measured in situ on STEREO-B: proton density (a), velocity, temp, plasma beta, and the magnetic-field, and pitch-angle distribution of suprathermal electrons quantified.b) mean charge of iron ions vs. solar radii, c) in situ measurements of the Fe-ion charge-state distribution.(Grechnev, et al,2019)

Based from (Rakowski, et al, 2007), in five out of eight sample CMEs the dominant Fe charge states are neon-like (16+) or higher, indicating that high temperatures, comparable to flares (107 K), are involved. Starting the plasma from this temperature and allowing the ions to recombine as they expand can often account for the Fe ionization balance, with peaks around Fe16 + and Fe8 + (the Ne-like and Ar-like charge states, which have small recombination rates to the next charge states down, hence population ‘‘bottlenecks’’ here). However, the lower Z elements place a limit on the maximum starting temperature (at least if assuming ionization equilibrium in the seed plasma). Above 106 K, O would be mainly O8 +, instead of O7 + and O6 + as observed, and would not recombine significantly during the CME evolution. Evidently plasma must start out much cooler, and be further heated as the CME accelerates.

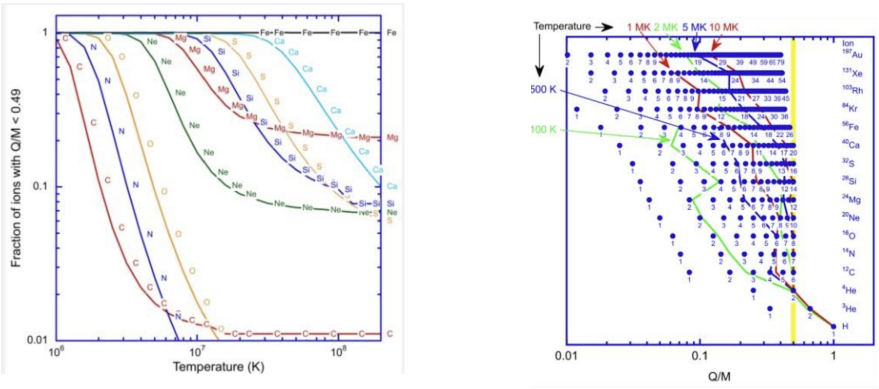

Figure a)Fraction of Elements which can be accelerated by waves below damped 4He Gyrofrequency waves. Flattening of curves at higher temperatures is from neutron rich isotopes outside gyrofrequency of damped waves. b) Charge to mass ratios of isotopes with coloured lines showing average ionisation state at temperatures, yellow bar shows Q/M =.5 where accelerating waves are damped by abundant 4He

The FIP-dependence of SEPs also differs from that of the solar wind; each has a different magnetic environment, where low-FIP ions and high-FIP neutral atoms rise toward the corona. Gradual energetic particles show strong fractionation relative to photospheric composition, with particles of first ionization potential (FIP) < 10 eV (also referred to as low-FIP elements) enhanced by approximately a factor of 2.7–3.5 relative to the photosphere. In these measurements, elements with FIP larger than 10 eV are depleted relative to O at approximately 80% and He at 50%.Two major sources generate SEPs: The small “impulsive” SEP events are associated with magnetic reconnection in solar jets that produce 1000-fold enhancements from H to Pb as a function of mass-to-charge ratio A/Q, and 1000X enhancements in 3He/4He. Ne/O is inversely correlated with wind speed, is nearly constant in the fast wind, and correlates strongly with solar activity in the slow wind. In fast wind streams with speeds above 600

km s−1, we find Ne/O = 0.10 ± 0.02, in good agreement with the extensive polar observations by Ulysses/SWICS. In slow wind streams with speeds below 400 km s−1, Ne/O ranges from a low of 0.12 ± 0.02 at solar maximum to a high of 0.17 ± 0.03 at solar minimum. (Shearar et al, 2014)

Solar-Terrestrial Relations Observatory (STEREO) mission addresses critical problems of the physics of explosive disturbances in the solar corona, interplanetary, and Earth. Paper describes IMPACT SEP package, the Suprathermal Ion Telescope (SIT) which identifies heavy ion composition(Mason, 2008) Further research may how trapped electrons (up to 7MeV+) in Van Allen belts with omnidirectional flux of 10^4-6 flux / cm^2 per sec electrons up to 4-8 Earth Radii could further neutralise CME and solar particles.

Event[a]	CME Speed[b] (km s^{-1})	CME Acceleration[b] (m s^{-2})	Final θ_{CME} (deg)	θ_{Flare} (deg)	Φ_{CME} (10^{21} Mx)	B_{Flare} (G)
1.....	660	58	41	2.2	3.5	490
2.....	850	61	64	27	8.7	8
3.....	2700	430	128	8.7	35	300

Table. Estimated Velocities, Angles, and Magnetic Quantities in Three CME Events in 2002 GOES X1, 1999, GOES X20 flare from (Moore, et al, 2007) from SOHO Lasco CME Catalog (Yashiro, et al, 2004)

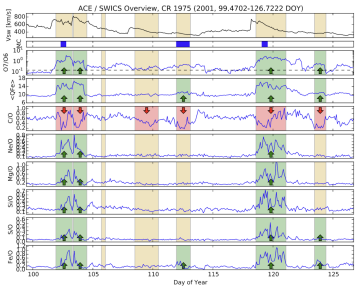

Figure 2. Solar wind plasma and composition measurements for a Carrington rotation in 2001. We use solar wind speed from SWICS; brown shaded time periods are indicative of ICME periods by Richardson and Cane. The blue shaded bars indicate the presence of magnetic cloud signatures identified in the same list. Ionic charge states of O and Fe are shown next, followed by the elemental compositional ratios of C/O, Ne/O, Mg/O, Si/O, S/O, and Fe/O. Significant increases and decreases of the elemental composition ratios are marked in green and red, respectively.

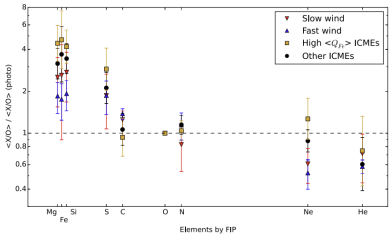

Figure 4. Elemental composition of compositionally hot ICMEs and other ICMEs as compared to the solar wind composition from fast, coronal hole-associated wind and from slow wind associated with streamers. Compositionally hot ICMEs have a higher FIP than both slow wind and other ICMEs. The Ne/O composition of hot ICMEs exceeds that of both slow and fast wind.

Figure. a) Solar Wind plasma and comparison measurements for carrington rotation in 2001. b) Elemental composition of hot iCMEs and other ICMEs compared to solar wind composition at fast, coronal hole and slow wind.